UNITED STATES
DEPARTMENT OF THE INTERIOR
GEOLOGICAL SURVEY

A STUDY OF FAULT PLANE MECHANISMS PRECEDING THE THANKSGIVING DAY, 1974 EARTHQUAKE AT HOLLISTER, CALIFORNIA

OPEN-FILE REPORT 78-255

This report is preliminary and has not been edited or reviewed for conformity with Geological Survey standards and nomenclature

Menlo Park, California
March, 1978

A STUDY OF FAULT PLANE MECHANISMS PRECEDING THE THANKSGIVING DAY, 1974 EARTHQUAKE AT HOLLISTER, CALIFORNIA

By David H. Warren

U. S. GEOLOGICAL SURVEY

OPEN-FILE REPORT 78-255

Menlo Park, California
March, 1978

ABSTRACT

Fault plane solutions were obtained for 80 microearthquakes in a 900 square km area centered on the Busch fault during a one year period preceding the Thanksgiving Day, 1974 Hollister earthquake. Strike slip motion occurred in 65 of the quakes, mainly at active spots on the Sargent, Castro, Busch, and Calaveras faults. There are 11 thrust-type and 4 normal-type solutions. No discernable rotation of compressional axes was observed to precede the Thanksgiving Day earthquake.

INTRODUCTION

The effort to predict earthquakes received a great impetus with the results of investigations by Nersesov and colleagues in central Asia (Nersesov et al, 1973). Among several features of the stress field before moderately strong earthquakes (magnitude 4.5 to 5.7), they reported a sudden rotation of the compressional stress axis in the micro-earthquake background, several months before the shock. One of their figures is reproduced here (Figure 1). The shift of interest shows as a sudden jump of about 100° from three to five months before three moderately strong earthquakes. The purpose of this paper is to see if such a rotation took place for a moderately strong earthquake in California. It is necessary to have a reasonably dense earthquake recording network operating continuously for the time period before the main shock.

The Geological Survey operates a dense network to detect micro-earthquakes in central California (Lester et al, 1976). As part of the processing to locate hypocenters for the earthquakes a spherical stereoplot is produced on the computer print-out which can be used to study the fault plane mechanism. The Thanksgiving Day earthquake of November 28, 1974, (magnitude 4.5) provided an opportunity to search for a rotation. This earthquake was located on the Busch fault (Rogers, 1967), just north of Hollister, California in a region where the USGS central California network had been operating since 1967. Aftershock locations and main-shock focal mechanism indicated left lateral motion along a nearly vertical fault striking N 33° E (W. H. K. Lee, unpublished manuscript).

A time period of one year was selected for study, from November 28, 1973 through November 28, 1974. A rectangular area centered on the Busch fault and extending 21 minutes in longitude and 15 minutes in latitude was searched using the SELECT computer program by Steppe (1976). For each earthquake selected the computer output from HYPO71 (Lee and Lahr, 1972) was examined to see whether a sufficient number of first motions (12) had been read to automatically generate a stereo plot. Of one hundred and two earthquakes with these plots, only eighty events had first motion data adequate for well-constrained focal plane solutions. Stations with reversed polarity were identified (Houck, 1976) and first motions corrected.

DATA ANALYSIS

A location map (Figure 2) shows the pattern of faulting taken from the Geologic map of California, San Jose sheet (Rogers, 1968) and Santa Cruz sheet (Jennings and Strand, 1958). Most faults trend northwest-southeast subparallel to the San Andreas fault. Near Hollister the San Andreas and Calaveras faults come close together, but apparently do not quite join. The Sargent fault, just south of Gilroy is a complicated fault having zones of imbrication (McLaughlin, 1971). It extends nearly to the Busch fault, and splinters into several more east-westerly trending faults which die out to the east, one of which is the Castro fault. The Busch fault (Rogers, 1967) forms an extensional feature between the Sargent and Calaveras faults.

Spherical stereo plots and solutions are shown (Figures 3-9) for the eighty earthquakes resolved. First motions are divided into compression or dilatation. The stereo plot was traced onto transparent paper and laid over an equal area grid to graphically find two perpendicular fault planes. It was assumed that the compressional and tensional axes are 45° from the fault planes. The compressional axes are shown in the figures. Whenever a solution had the compressional axis in the southern quadrant the northward direction of the axis is given in parenthesis. The northward direction is desired for the azimuth comparisons to follow. Table 1 lists parameters for all earthquakes and uses a number key to identify the solutions. The mechanisms of the solutions and their locations are shown on a separate map (Figure 10).

The azimuth of compressional axes is plotted as a function of time (Figure 11). Earthquakes are coded by fault location for the one year period selected. An event was required to be within one kilometer of the fault in order for it to be identified with that fault. Otherwise it was classified as not on known faulting. A moderate earthquake (magnitude 4) occurred on Jan. 10, 1974 and initiated a prolonged period of activity on the Castro fault. The plot shows no discernible change in direction of axes for either the entire area or for any of the faults.

From the location of the earthquakes (Figure 10) it can be seen that most are on a series of hot spots that trend northwest-southeast across the area. This trend appears on a seismicity map by Lee et al. (1972). Most of the earthquakes are located on the Sargent and Castro faults. There are 27 events clustered in the composite solution shown on the Castro fault. Other hot spots are on the Busch fault and the Calaveras fault. Many of the remaining earthquakes are located at known faults, while some quakes are not and contribute to the diffuse background of seismicity.

The fault plane solutions in figures 3 through 9 show the type of motion. Of the eighty solutions, sixty-five show strike-slip motion, eleven show thrusting, and four show normal fault motion. One event shows purely vertical motion. Table 2 shows a comparison of directions obtained from the fault plane solutions with azimuth measured from the map of faulting. A simple average of azimuth of compressional axes was calculated for strike-slip motions on the fault. Then 45° was added or subtracted to obtain the azimuth of fault plane. The actual fault

azimuth, as measured from the geologic map, is shown for comparison. The comparison shows excellent agreement for the Sargent and Castro faults and the agreement is not as good for the Busch and Calaveras faults. The Sargent, Castro, and Calaveras faults exhibit right lateral strike slip, while the Busch fault shows left lateral motion.

A measure of the precision of the orientation of compressional axes was estimated by noting how far the axes of the solution can be rotated without violating much of the pattern. About a third of the strike-slip solutions were selected, then the stereo plot for each was rotated back and forth over the equal area grid and the angle noted that results in two points changing quadrants. The angle averaged 9° but varied from 0 to 16°. This might be considered a limit of error because the pattern is seriously violated at the extremes. From these considerations, the probable error is estimated to average about five degrees, but may vary from solution to solution.

CONCLUSIONS

This study of one year of microearthquakes preceding the Thanksgiving Day, 1974 Hollister earthquake shows no discernable rotation of strain axes preceding the quake, of the type proposed by Russian investigators.

The fault plane mechanisms show that most micro-earthquakes exhibit strike-slip motion occurring on the Sargent, Castro, Busch, and Calaveras faults. Motion is right lateral on the Sargent, Castro, and Calaveras faults, and left lateral on the Busch fault.

Acknowledgement

Charles Bufe selected the target area of this investigation and provided quidance and encouragement during its execution. Frederick Lester and the staff of the central California network provided the data used.

References

Houck, T., J. Guerrero, A. Miller, and W. H. K. Lee, 1975, 1974 Handbook for U.S.G.S. central California microearthquake network: U.S. Geological Survey Open-File Report 75-397, 37 p.

Jennings, C. W., and R. G. Strand, 1958, Geologic map of California, Santa Cruz sheet, Olaf P. Jenkins edition: Div. of Mines and Geology, Sacramento, Calif.

Lee, W. H. K., and J. C. Lahr, 1972, HYPO71: A computer program for determining hypocenter, magnitude, and first motion pattern of local earthquakes: U.S. Geological Survey Open-File Report, 100 p.

Lee, W. H. K., J. C. Roller, K. L. Meagher, P. G. Bauer, R. E. Bennett, J. V. Johnson, E. E. Matamoros, and R. D. Brown, Jr., 1972 Seismicity map of Greater San Francisco Bay Area, California, 1969-71,: U.S. Geological Survey Map, 1 sheet.

Lester, F. W., S. L. Kirkman, and K. L. Meagher (1976), Catalog of earthquakes along the San Andreas fault system in central California, October-December 1973: U.S. Geological Survey Open-File Report 76-732, 36 p.

McLaughlin, R. J., 1971, Geologic map of the Sargent Fault Zone in the vicinity of Mount Madonna, Santa Clara County, California: San Francisco Bay Region Environment and Resources Planning Study, Basic data contribution 13, U.S. Geological Survey Open File Map.

Nersesov, I. L., A. A. Lukk, V. S. Ponomarev, T. G. Rautian, B. G. Rulev, A. N. Semenov, and I. G. Simbireva, 1973, Possibilities of earthquake prediction, exemplified by the Garm area of the Tadzhik S. S. R.: Moscow, Akad. Nauk. SSSR Inst. Fiziki Zemli, p. 72-99.

Rogers, T. H., (1966) Geologic map of California, San Jose sheet, Olaf P. Jenkins edition: Div. of Mines and Geology, Sacramento, Calif.

Rogers, T. H., 1967, Active extensional faulting north of Hollister near the Calaveras fault zone., Bull. Seism. Soc. Am., v. 57, p. 813-816.

Steppe, J. A. (1976), Select, extract, setup: A set of computer programs for searching and modifying local earthquake data: U.S. Geological Survey Open-File Report 76-342, 70 p.

TABLE 1

No. Key	1973 or 1974 Date	Time	Latitude Deg.	Latitude Min.	Longitude Deg.	Longitude Min.	Depth (km)	Mag.	Type of Faulting	Azimuth of compressional axis (deg.)	Dip of compressional axis (deg.)	Fault
1	11/29	0632	36	46.41	121	26.61	7.2	1.3	Thrust	237 (57)	5	P
2	11/30	0415	36	54.04	121	34.38	3.9	1.5				P
3	12/3	2020	36	58.36	121	38.83	5.1	1.4	Strike-slip	343	0	G
4	12/5	2308	36	58.71	121	27.09	4.5	2.2	Strike-slip	22	0	C
5	12/10	1829	36	55.87	121	33.00	4.4	2.0	Strike-slip	344	0	O
6	12/11	0735	36	53.65	121	24.70	8.1	2.9	Strike-slip	216 (36)	22	C
7	12/12	1051	36	47.85	121	18.53	9.5	1.4				P
8	12/12	1430	36	56.41	121	33.66	5.0	1.1	Strike-slip	356	14	O
9	12/13	0217	36	48.64	121	23.68	7.6	2.7	Strike-slip	197 (17)	14	O
10	12/14	1119	36	56.00	121	25.10	7.2	1.8				P
11	12/15	2314	36	50.15	121	34.00	5.6	1.7	Thrust	352	30	O
12	12/16	0332	36	50.99	121	34.72	4.3	1.8	Strike-slip	1	17	P
13	12/21	0917	36	53.10	121	24.37	6.7	1.3	Thrust	5	12	C
14	1/6	0235	36	57.15	121	37.98	5.2	1.7	Thrust	211 (31)	3	P
15A	1/10	1122	36	57.08	121	35.78	7.8	3.9				S
15	1/10	1144	36	57.04	121	35.48	5.8	1.7	Strike-slip	148 (328)	28	S
16	1/10	1429	36	57.16	121	35.47	6.6	2.0	Strike-slip	156 (336)	27	S

TABLE 1 (continued)

No. Key	1974 Date	Time	Latitude Deg.	Latitude Min.	Longitude Deg.	Longitude Min.	Depth (km)	Mag.	Type of Faulting	Azimuth of compressional axis (deg.)	Dip of compressional axis (deg.)	Fault
17	1/13	2249	36	57.20	121	35.74	7.3	2.6				S
18	1/15	1026	36	57.18	121	35.66	6.4	1.7	Strike-slip	155 (335)	27	S
19	1/15	1027	36	57.20	121	35.66	5.5	1.9	Strike-slip	153 (333)	20	S
20	1/15	2048	36	57.03	121	35.05	6.4	1.4	Thrust	356	2	S
21	1/16	0116	36	56.88	121	35.16	5.8	1.4	Strike-slip	332	0	S
22	1/18	1303	36	57.02	121	35.42	5.9	1.4	Strike-slip	352	0	S
23	1/20	1517	36	53.25	121	24.59	7.4	1.7	Strike-slip	217 (37)	21	C
24	1/21	1451	36	57.07	121	35.55	5.9	1.5	Thrust	342	0	S
25	1/30	0051	36	57.02	121	35.53	6.0	1.2	Thrust	341	0	S
26	1/30	0235	36	57.02	121	35.36	5.1	1.0				S
27	2/1	0430	36	47.94	121	31.71	6.4	0.9				P
28	2/1	1815	36	48.08	121	32.20	6.5	1.5				O
29	2/8	0215	36	56.17	121	33.31	4.8	2.7	Strike-slip	163 (343)	14	O
30	2/12	0835	36	51.95	121	19.53	9.3	1.8	Strike-slip	13	14	C
31	2/15	0237	36	51.29	121	27.55	2.5	1.6	Strike-slip	164 (344)	14	P
32	2/25	0857	36	57.19	121	35.66	5.6	2.0	Strike-slip	156 (336)	21	S
33	3/7	0437	36	51.99	121	20.20	5.6	1.2	Strike-slip	44	0	P

TABLE 1 (continued)

Kn. Key	1974 Date	Time	Latitude Deg.	Latitude Min.	Longitude Deg.	Longitude Min.	Depth (km)	Mag.	Type of Faulting	Azimuth of compressional axis (deg.)	Dip of compressional axis (deg.)	Fault
34	3/7	1454	36	57.11	121	35.48	5.3	2.3	Strike-slip	157 (337)	13	S
35	3/13	0851	36	56.95	121	35.23	5.7	1.3	Strike-slip	338	0	S
36	3/31	2309	36	57.15	121	35.68	4.1	2.2				S
37	4/1	1119	36	56.93	121	35.34	4.9	1.8	Strike-slip	135 (315)	28	S
38	4/10	1713	36	56.94	121	35.73	4.6	2.5				S
39	4/10	2205	36	56.78	121	35.59	4.6	1.9				S
40	4/12	0020	36	57.13	121	35.71	4.4	2.0	Strike-slip	143 (323)	21	S
41	4/12	1328	36	55.25	121	34.04	6.5	1.4	Strike-slip	188 (8)	27	G
42	4/12	1338	36	55.23	121	33.37	6.5	1.4	Strike-slip	172 (352)	36	G
43	4/12	1400	36	58.11	121	38.44	5.3	2.0				G
44	4/17	1949	36	57.05	121	35.64	4.4	1.5				S
45	4/17	2022	36	57.04	121	35.57	4.8	1.8	Strike-slip	135 (315)	29	S
46	4/17	2234	36	57.04	121	35.68	4.7	1.4				S
47	4/18	0703	36	57.13	121	35.70	4.7	1.9	Strike-slip	138 (318)	7	S
48	4/18	0740	36	57.08	121	35.80	4.7	1.4	Strike-slip	138 (318)	26	S
49	4/18	1015	36	57.09	121	35.36	3.7	0.8	Strike-slip	140 (320)	46	S
50	4/20	0830	36	56.81	121	35.48	3.6	1.7	Thrust	165 (345)	36	S

TABLE 1 (continued)

No. Key	1974 Date	Time	Latitude Deg.	Latitude Min.	Longitude Deg.	Longitude Min.	Depth (km)	Mag.	Type of Faulting	Azimuth of compressional axis (deg.)	Dip of compressional axis (deg.)	Fault
51	4/20	2005	36	57.16	121	35.92	3.5	1.4	Strike-slip	159 (339)	14	S
52	5/14	0830	36	53.22	121	29.76	3.6	1.4				O
53	5/21	1209	36	54.94	121	28.71	4.6	1.7	Strike-slip	175 (355)	4	B
54	5/23	0729	36	55.04	121	28.65	5.0	1.0	Strike-slip	3	0	B
55	5/30	0127	36	58.06	121	38.48	3.4	1.9	Strike-slip	346	8	G
56	6/11	1747	36	57.83	121	38.28	5.0	1.6				G
57	6/14	1038	36	54.10	121	24.10	8.0	1.0	Strike-slip	5	28	P
58	6/16	0538	36	55.02	121	28.20	5.0	1.4				B
59	6/16	1737	36	55.28	121	28.52	5.0	1.7				B
60	6/17	1138	36	51.99	121	24.78	4.7	2.4	Strike-slip	38	0	C
61	6/17	1511	36	57.38	121	36.89	5.0	1.6	Normal	41	84	G
62	6/19	0132	36	57.69	121	37.98	4.8	1.6	Strike-slip	340	0	G
63	6/20	0904	36	52.88	121	24.90	6.1	2.8	Vertical	262 (82)	45	C
64	6/26	1033	36	53.89	121	24.16	6.7	1.2				P
65	6/26	1141	36	52.12	121	24.68	4.8	1.6				C
66	7/2	0733	36	56.91	121	34.98	3.5	1.7	Strike-slip	342	0	S
67	7/2	0800	36	56.89	121	35.07	4.4	1.9				S

TABLE 1 (continued)

No. Key	1974 Date	Time	Latitude Deg.	Latitude Min.	Longitude Deg.	Longitude Min.	Depth (km)	Mag.	Type of Faulting	Azimuth of compressional axis (deg.)	Dip of compressional axis (deg.)	Fault
68	7/6	0521	36	54.77	121	28.41	5.9	1.5	Strike-slip	338	0	B
69	7/15	2341	36	52.43	121	36.35	4.8	1.6				P
70	7/20	0553	36	54.87	121	31.39	4.0	1.4	Strike-slip	188 (8)	28	O
71	7/29	1823	36	48.94	121	28.06	10.2	1.0	Thrust	41	25	P
72	8/8	0646	36	52.97	121	24.46	7.5	1.4	Strike-slip	216 (36)	29	C
73	8/16	1618	36	51.87	121	19.67	5.0	1.7	Strike-slip	11	6	P
74	8/17	0315	36	53.64	121	23.65	8.5	1.3	Thrust	215 (35)	6	P
75	8/17	2259	36	57.38	121	36.12	6.5	1.5	Normal	33	82	S
76	8/20	1825	36	48.44	121	23.69	7.4	2.1	Strike-slip	20	0	P
77	8/25	1715	36	57.76	121	37.84	4.6	2.0	Strike-slip	343	0	G
78	8/29	0237	36	56.91	121	35.00	5.8	1.7	Strike-slip	344	0	S
79	8/30	0755	36	49.62	121	21.03	6.1	2.8	Strike-slip	173 (353)	20	P
80	9/8	1020	36	52.99	121	31.69	4.5	1.9	Strike-slip	342	14	P
81	9/11	0703	36	58.04	121	37.93	1.6	1.9	Strike-slip	357	9	G
82	9/13	1751	36	48.69	121	24.25	7.8	1.6	Thrust	13	2	P
83	9/14	0321	37	2.13	121	28.52	8.1	1.2	Strike-slip	45	0	P
84	9/18	0744	36	48.65	121	24.36	8.3	1.1	Strike-slip	348	29	P
85	9/19	0747	37	2.06	121	28.70	7.8	1.2	Strike-slip	52	22	P

TABLE 1 (continued)

No. Key	1974 Date	Time	Latitude Deg.	Latitude Min.	Longitude Deg.	Longitude Min.	Depth (km)	Mag.	Type of Faulting	Azimuth of compressional axis (deg.)	Dip of compressional axis (deg.)	Fault
86	9/26	0037	36	53.07	121	32.98	6.5	1.6	Normal	330	66	P
87	9/27	1616	37	2.10	121	28.82	8.3	2.0	Strike-slip	54	0	P
88	9/28	0632	36	57.36	121	36.48	5.2	1.8	Strike-slip	331	0	S
89	10/5	2243	36	57.89	121	37.41	6.0	1.7	Normal	240 (60)	75	G
90	10/6	0413	36	49.91	121	34.04	6.1	2.1	Strike-slip	348	20	O
91	10/7	0130	36	56.96	121	35.64	4.5	1.8	Strike-slip	332	0	S
92	10/10	0639	36	57.95	121	38.48	4.5	1.7	Strike-slip	3	14	G
93	10/14	1039	36	57.06	121	35.57	5.5	2.1	Strike-slip	164 (344)	14	S
94	10/21	0607	36	57.98	121	38.46	5.0	2.0	Strike-slip	347	0	G
95	10/28	0604	36	53.41	121	24.72	8.2	1.9	Strike-slip	212 (32)	14	C
96	10/31	2212	36	57.16	121	35.57	5.9	1.6	Strike-slip	357	0	S
97	11/2	1613	36	50.22	121	24.47	10.3	2.0	Strike-slip	32	14	P
98	11/14	2129	36	54.89	121	28.52	5.2	1.5	Strike-slip	344	0	B
99	11/20	0908	36	50.25	121	24.74	5.3	1.6	Strike-slip	352	6	P
100	11/24	0751	36	56.98	121	35.37	6.1	1.5	Strike-slip	356	0	S
101	11/28	2301	36	54.95	121	28.63	5.5	4.5	Strike-slip	355	0	B

Faults on which earthquakes occur are coded as follows:
B, Busch fault; C, Calaveras fault; G, Sargent fault;
S, Castro fault; O, other known faulting; P, not on known faulting.

Table 2

Azimuth, degrees

Average of Compressional Axis	45° from Average of Compressional Axis	Northward Fault	Fault Name
349	304	307	Sargent
334	289	291	Castro
350	35	41	Busch
39	346	339	Calaveras

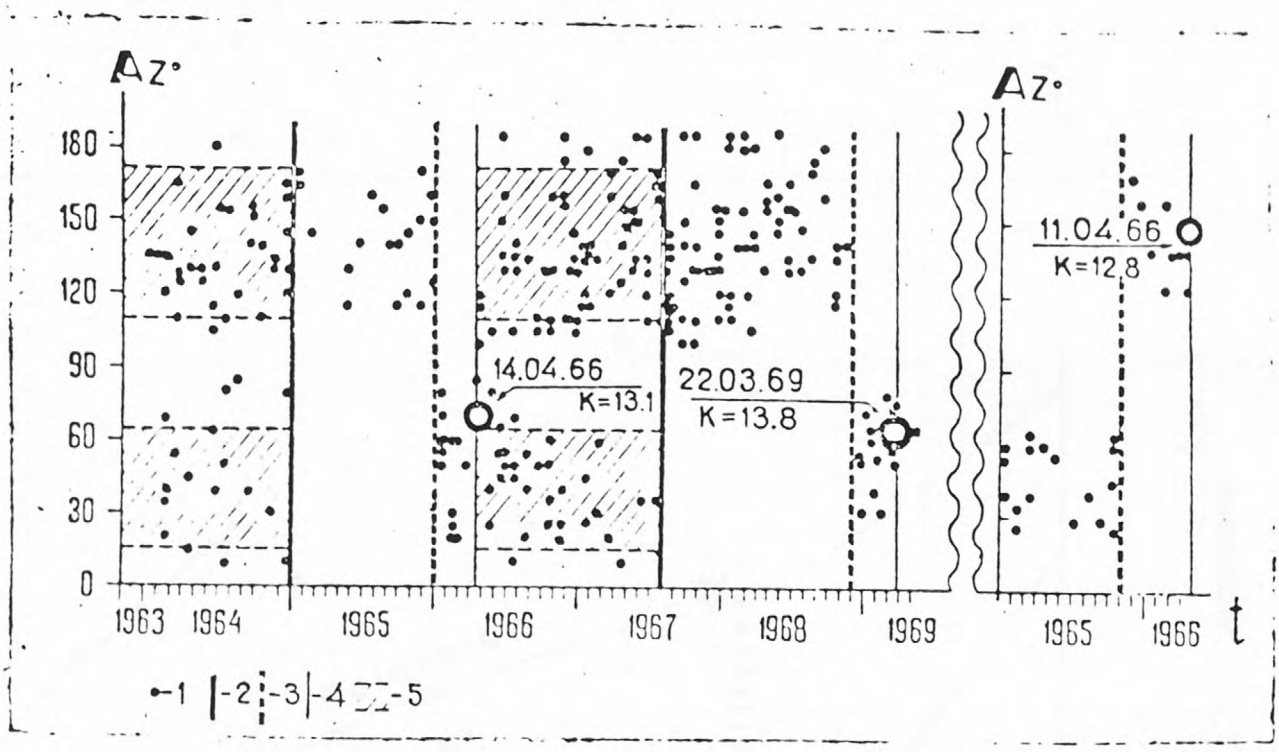

Figure 1. Reproduced from Nersesov et al. (1973). Reorientation of the principal axes of compressional stress in the foci of weak earthquakes in the fourth sector before strong shocks.
1)- azimuths of orientation of axes of compression;
2)- boundaries of existence of two preferred directions of orientation of axes of compression;
3)- region of rearrangement of orientation of axes of compression--"short-term";
4)- ditto, "long-term".

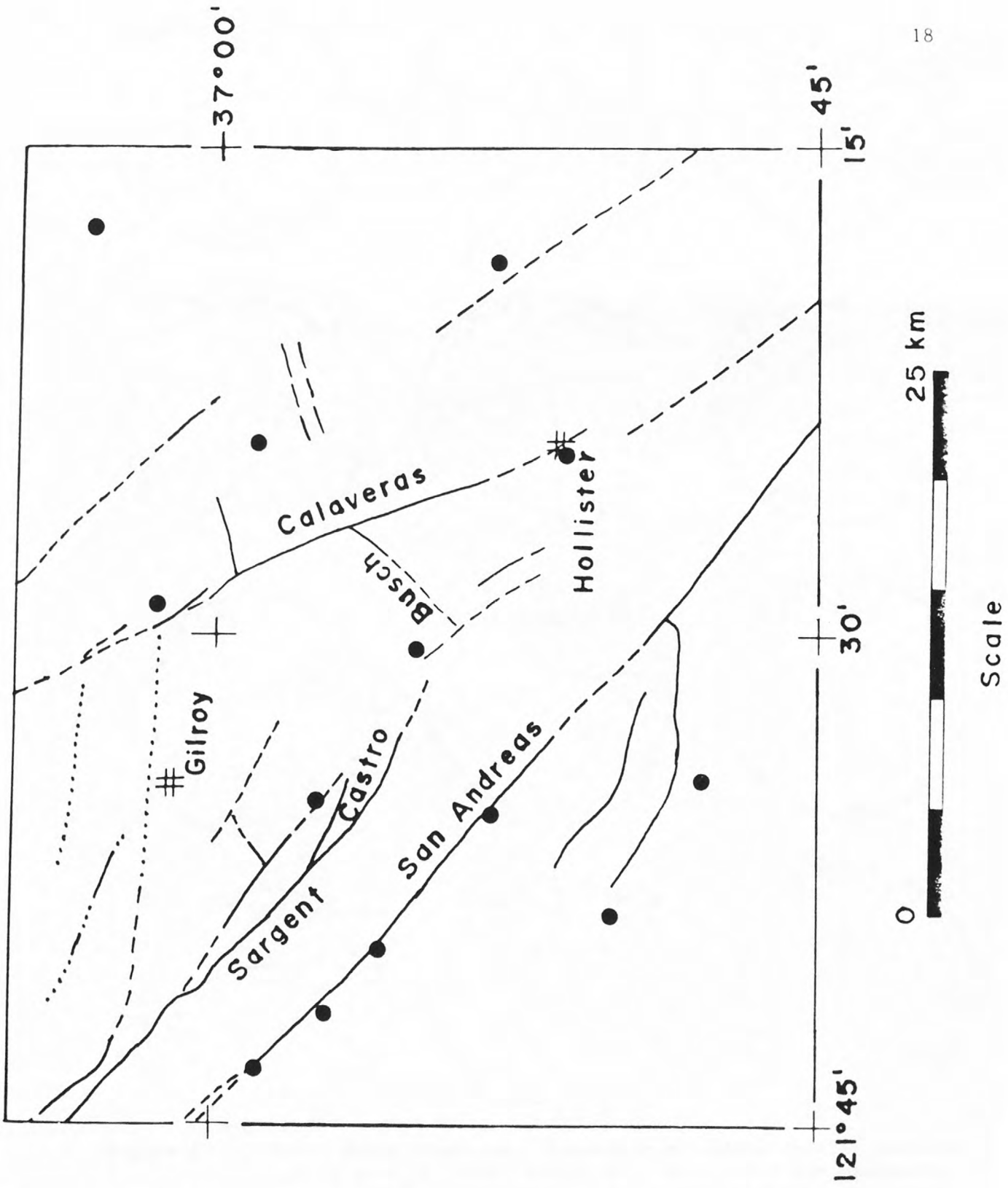

Figure 2. Location map, showing the area of California of this study. Faulting is taken from the Geologic Map of California, San Francisco and San Jose sheets. Solid circles show stations of the central California network.

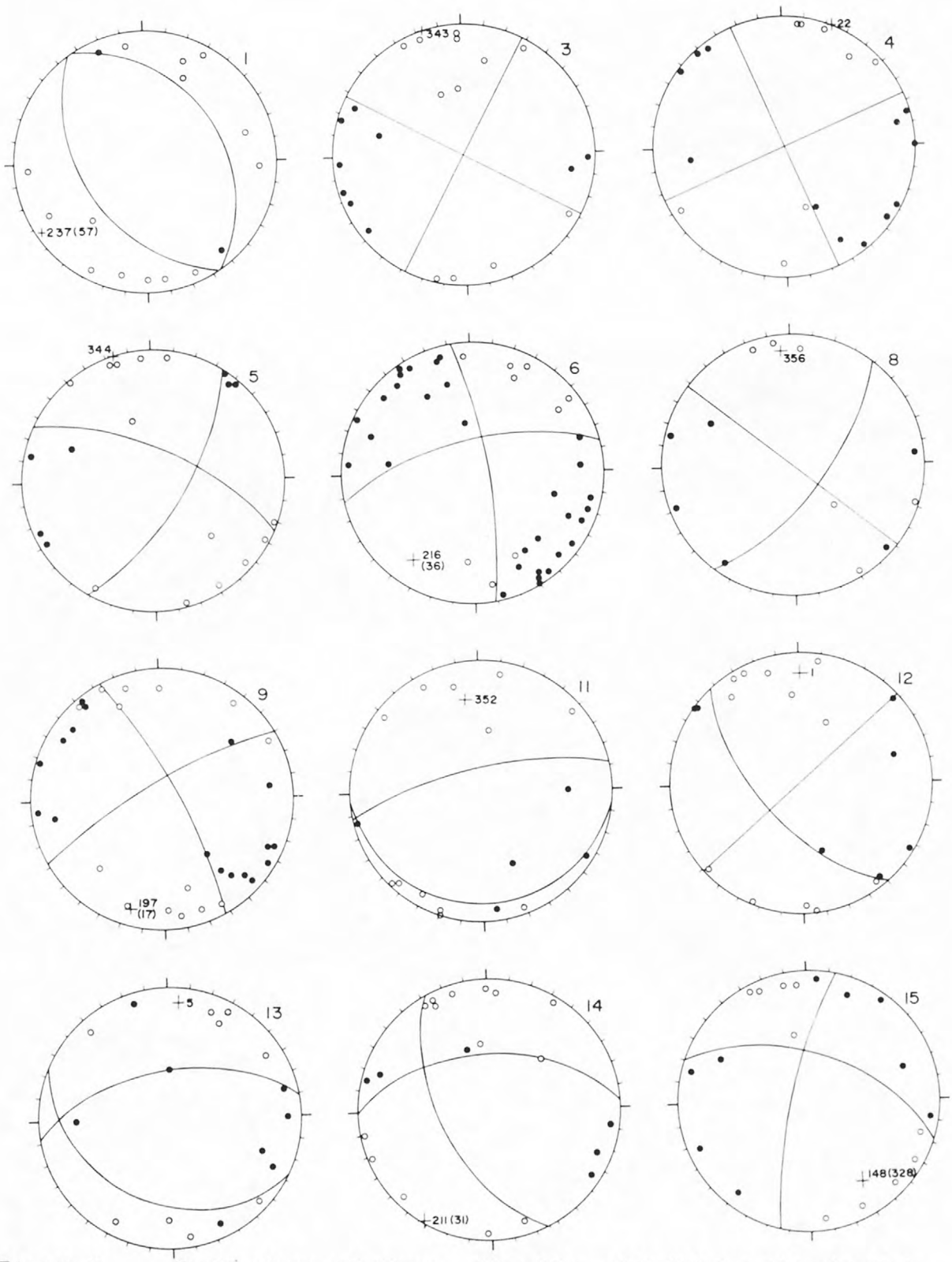

Figure 3. Fault plane solutions. Direction of initial motion is plotted on an equal area stereo net. Closed circles represent compression and open circles represent dilation. The projections of the planes of solution are shown as curved lines. The compressional axis is shown by a cross and the azimuth is given, in parentheses if it is reciprocal.

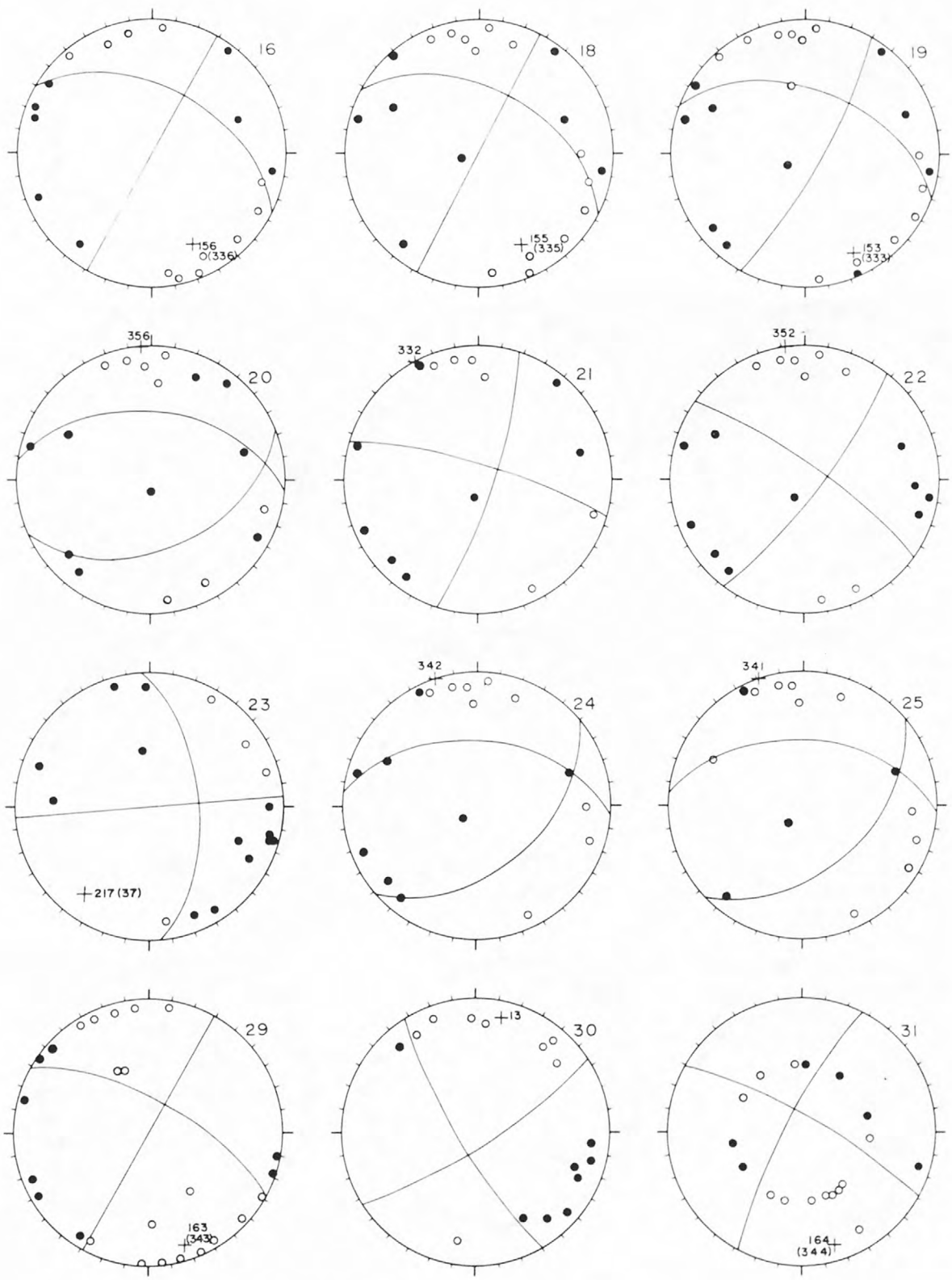

Figure 4. See caption for Figure 3.

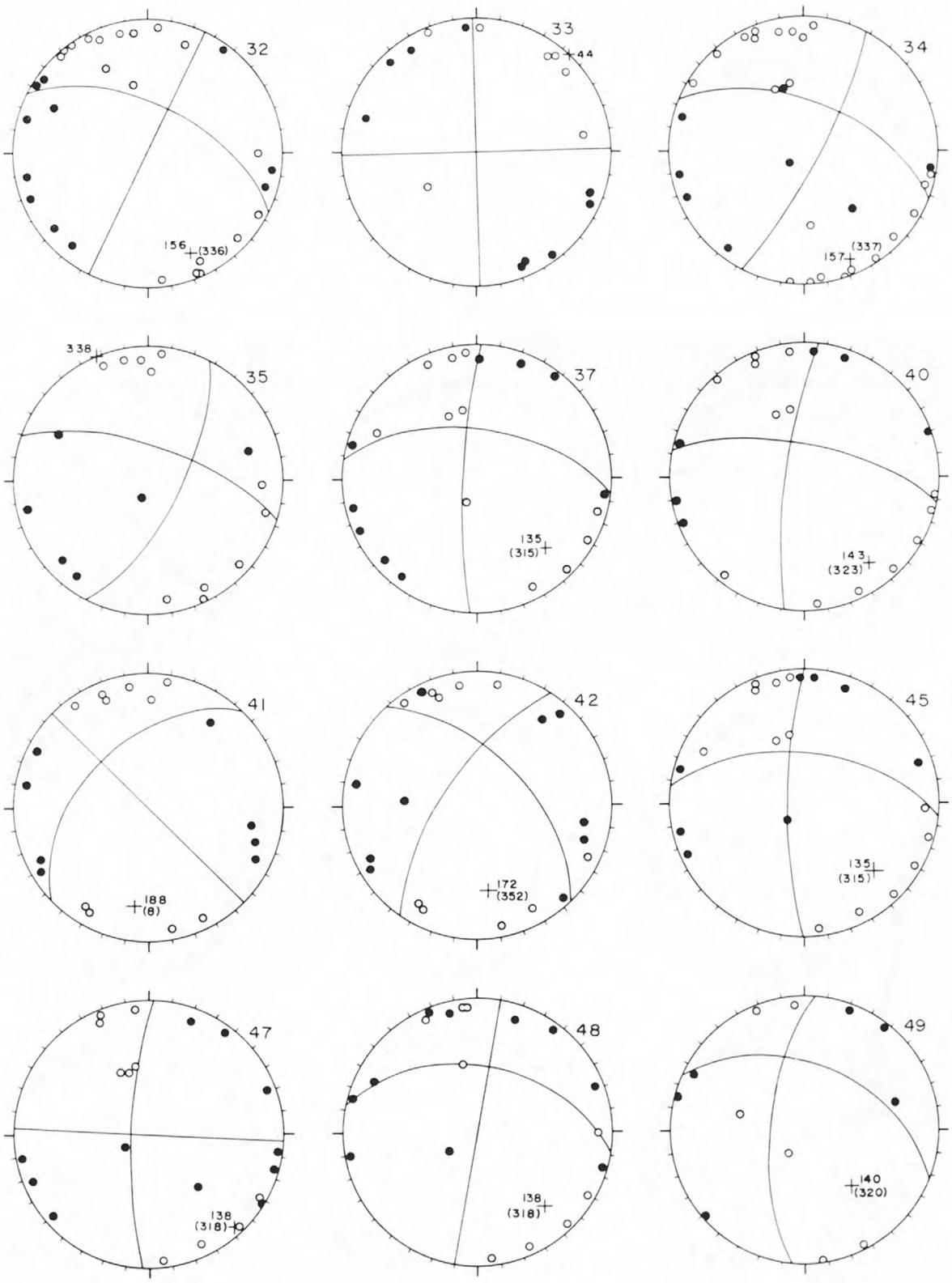

Figure 5. See caption for Figure 3.

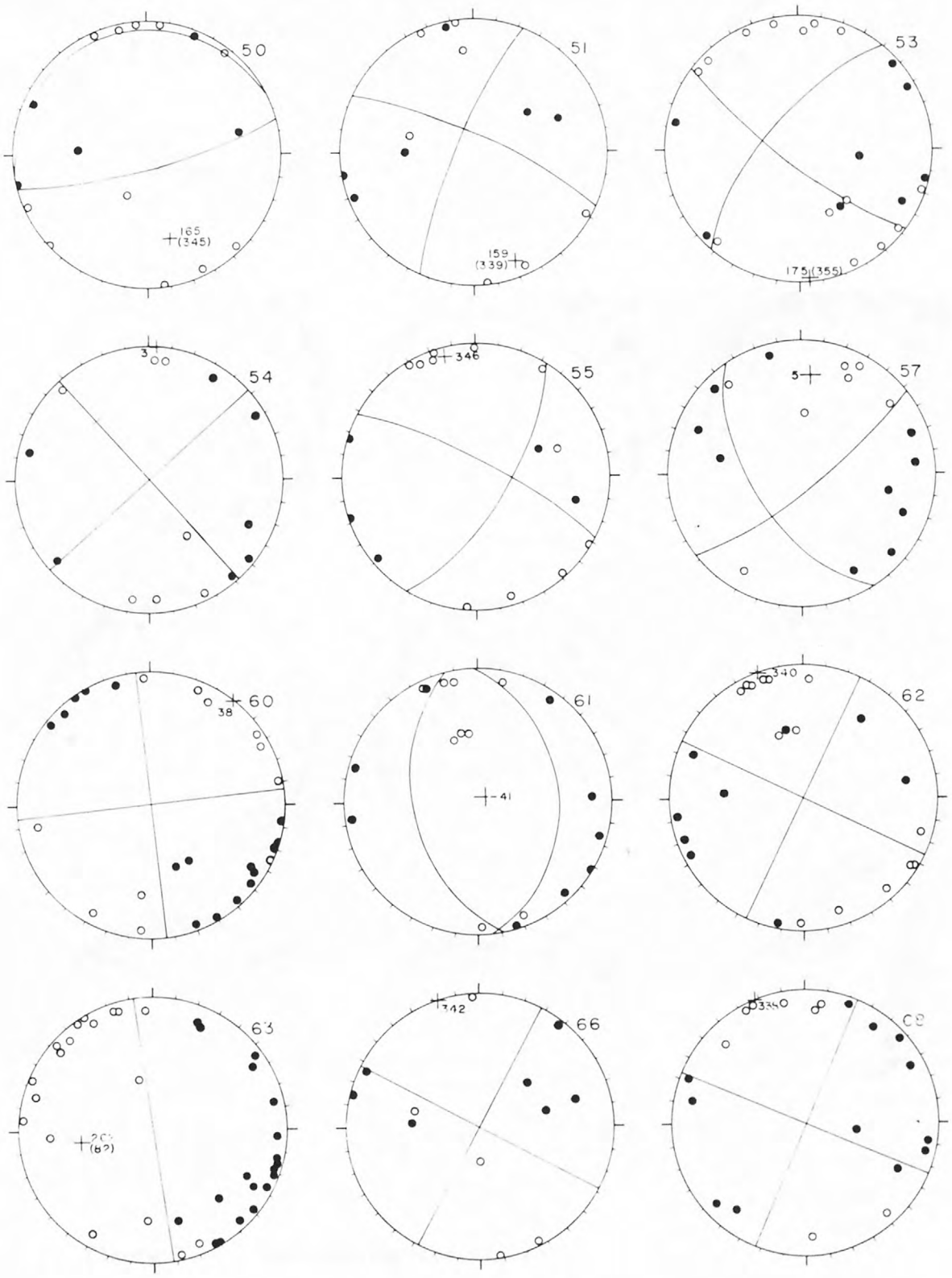

Figure 6. See caption for Figure 3.

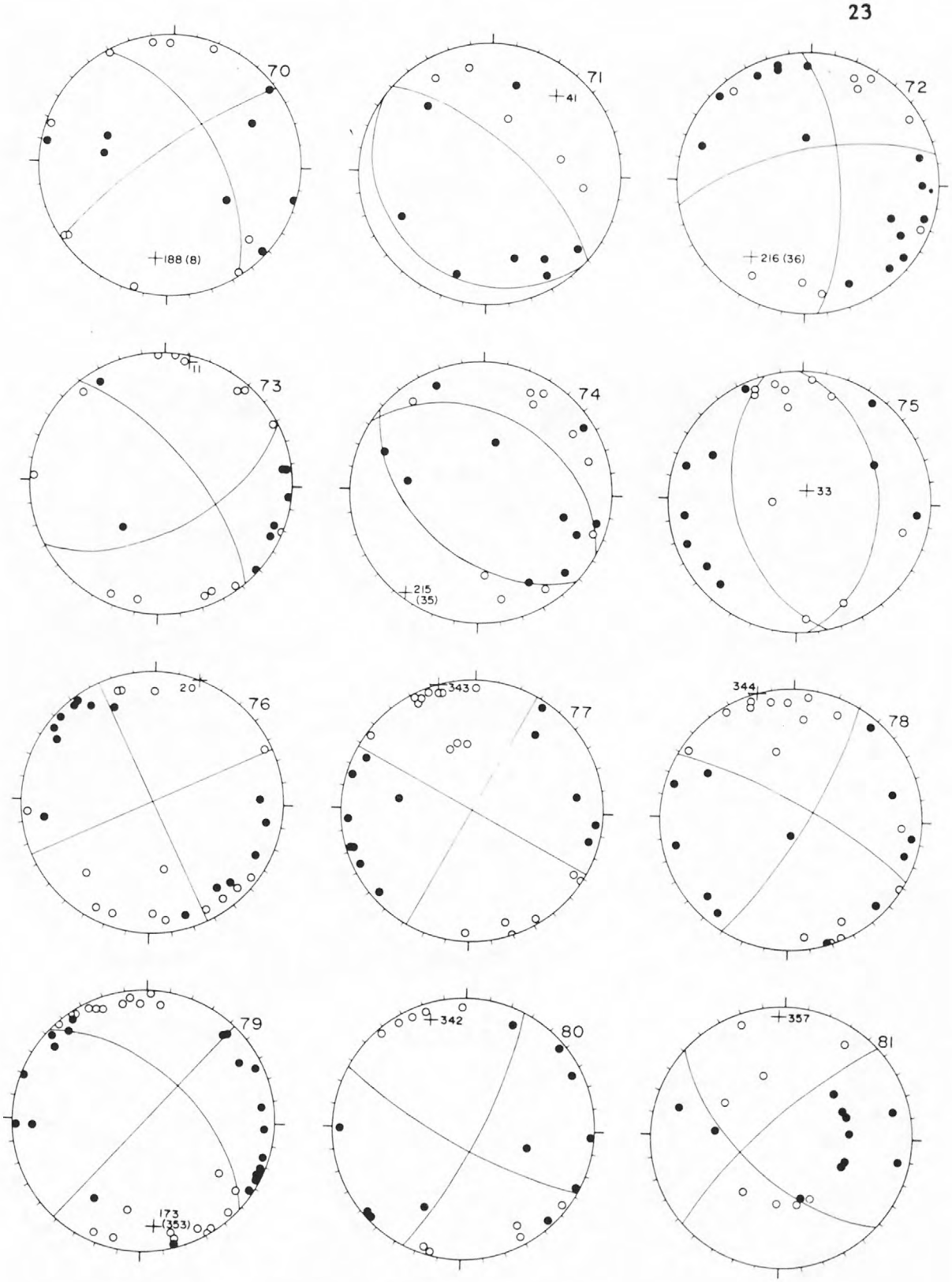

Figure 7. See caption for Figure 3.

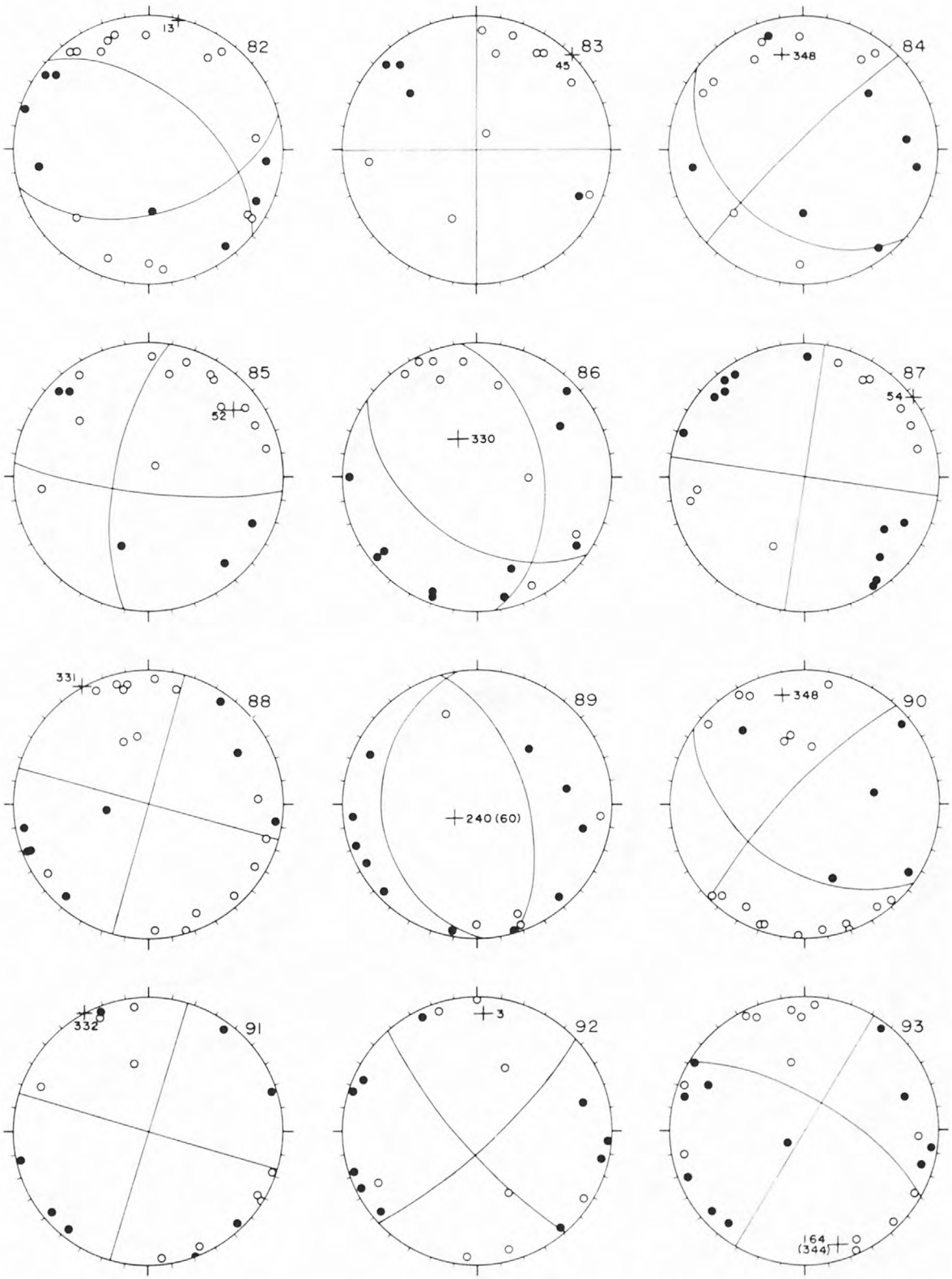

Figure 8. See caption for Figure 3.

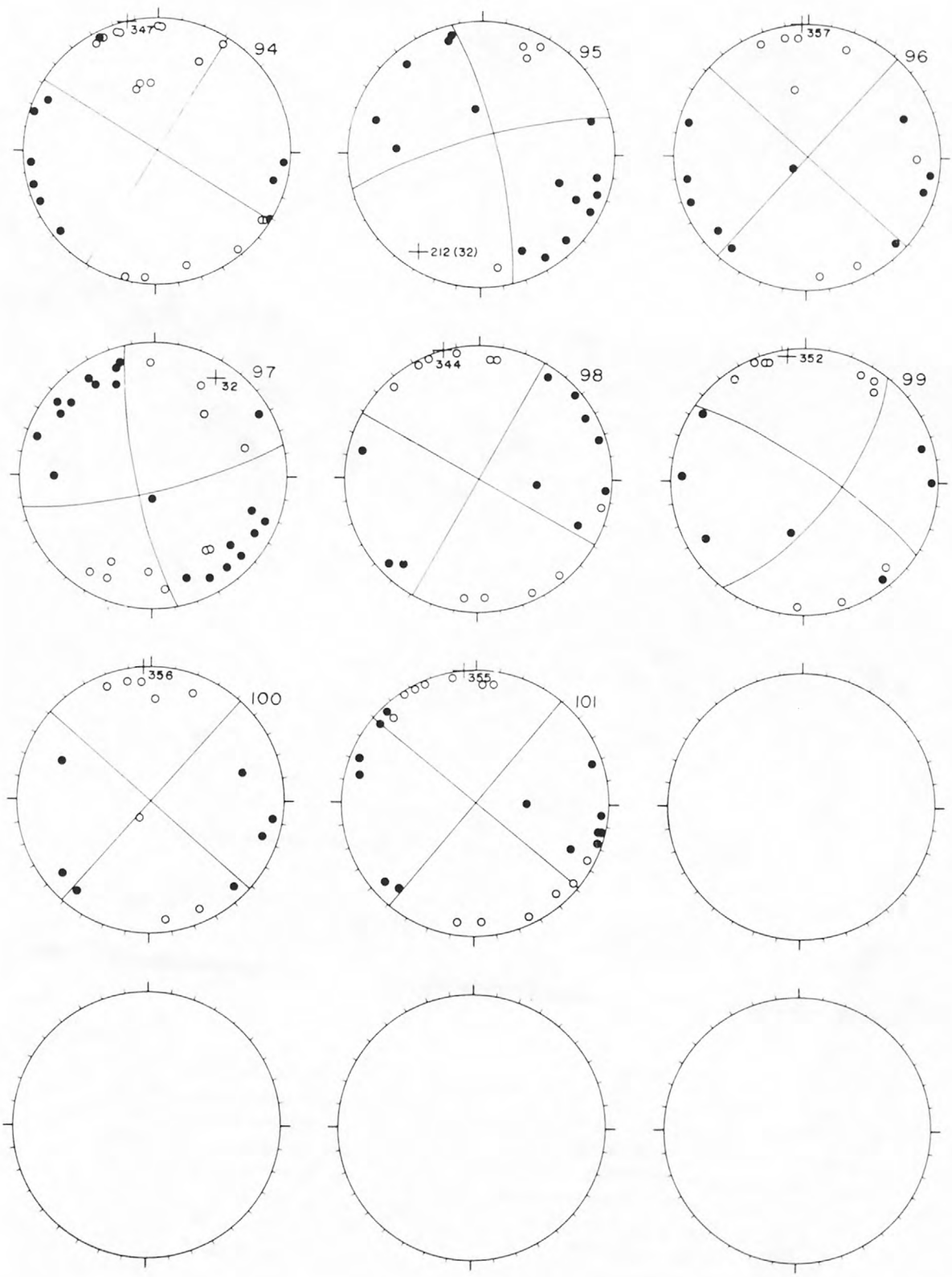

Figure 9. See caption for Figure 3.

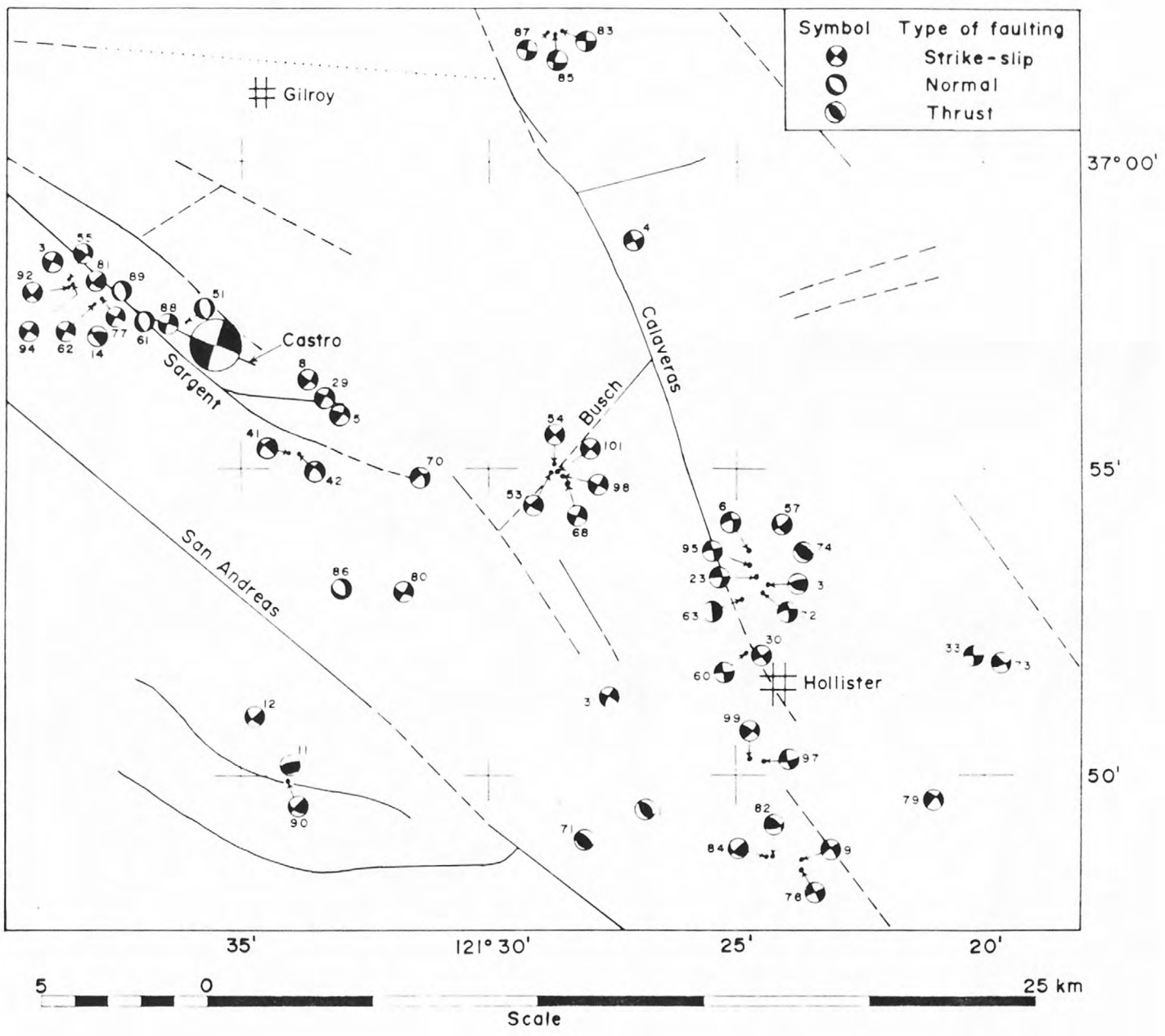

Figure 10. Fault mechanism map from November 1973 through November 1974. Faulting is from the Geologic Map of California, San Francisco and San Jose sheets. Compressional quadrants are shown as black areas and dilatational quadrants are shown as open areas within the circles, separated by the nodal planes. The large circle on the Castro fault encloses a composite solution of 22 strike-slip events. Within this circle there were also four thrust events and one normal event.

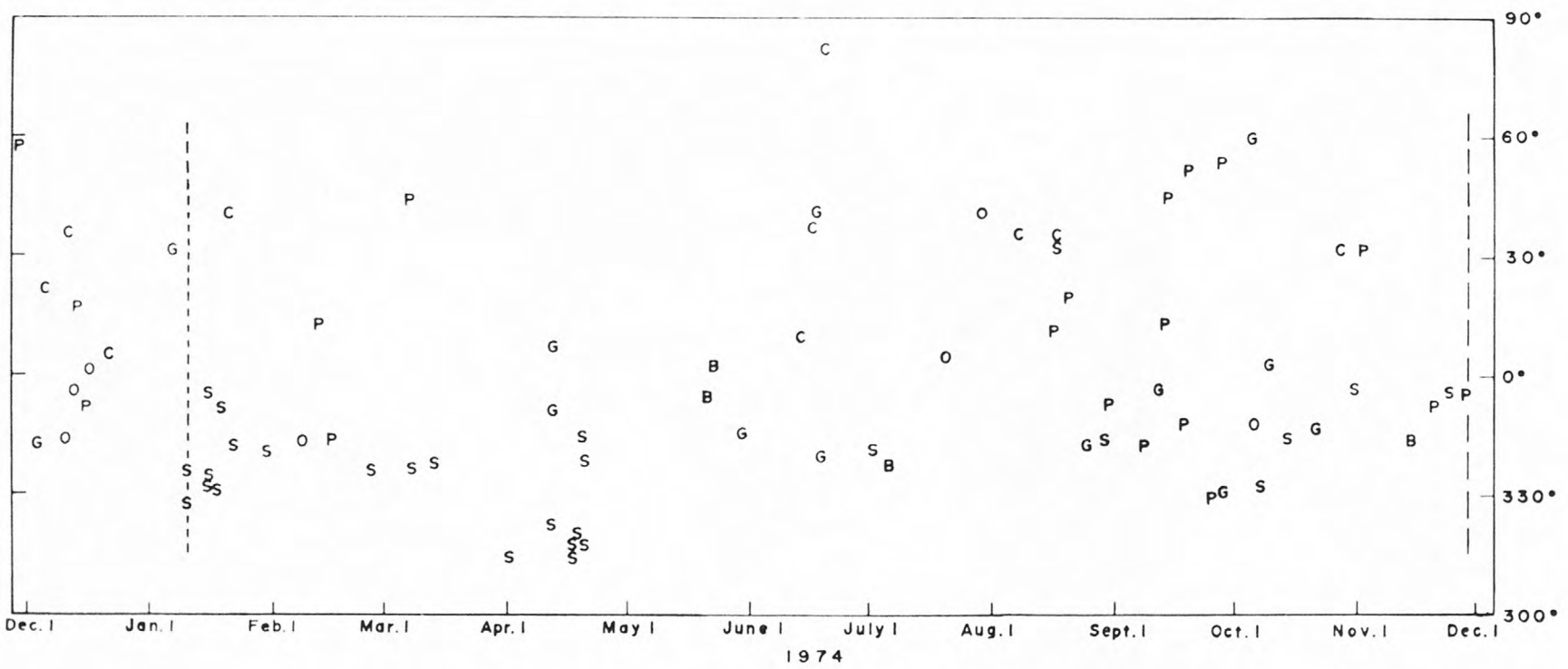

Figure 11. Plot of azimuth of the pole of compressional axis as a function of time. Letters represent earthquakes on faults, as follows: B, Busch fault; C, Calaveras fault; G, Sargent fault; S, Castro fault; O, other known faulting; P, not on known faulting.